Published in final edited form as:
J Comp Neurol. 2014 March ; 522(4): 921–936. doi:10.1002/cne.23453.

Electron Tomography on γ-Aminobutyric Acid-ergic Synapses Reveals a Discontinuous Postsynaptic Network of Filaments

Alexander E. Linsalata[1], **Xiaobing Chen**[1], **Christine A. Winters**[1], and **Thomas Reese**[1]
[1]Lab of Neurobiology, NINDS, NIH, Bethesda, MD 20892, USA

Abstract

The regulation of synaptic strength at γ-aminobutyric acid (GABA)-ergic synapses is dependent on the dynamic capture, retention, and modulation of GABA A-type receptors by cytoplasmic proteins at GABAergic postsynaptic sites. How these proteins are oriented and organized in the postsynaptic cytoplasm is not yet established. In order to better understand these structures and gain further insight into the mechanisms by which they regulate receptor populations at postsynaptic sites, we utilized electron tomography to examine GABAergic synapses in dissociated rat hippocampal cultures. GABAergic synapses were identified and selected for tomography using a set of criteria derived from the structure of immunogold-labeled GABAergic synapses. Tomography revealed a complex postsynaptic network composed of filaments that extend ∼100 nm into the cytoplasm from the postsynaptic membrane. The distribution of these postsynaptic filaments was strikingly similar to that of the immunogold label for gephyrin. Filaments were interconnected through uniform patterns of contact, forming complexes composed of 2-12 filaments each. Complexes did not link to form an integrated, continuous scaffold, suggesting that GABAergic postsynaptic specializations are less rigidly organized than glutamatergic postsynaptic densities.

Keywords

inhibitory synapse; postsynaptic density; gephyrin; γ-aminobutyric acid receptor; glycine receptor

Introduction

Rapid neurotransmission relies on the concentration of ligand-gated ionotropic receptors at postsynaptic sites. In addition, modulation of the number of receptors at these sites is a common mechanism for regulating the strength and shape of postsynaptic responses throughout the nervous system (Balice-Gordon and Lichtman, 1993; Gaiarsa et al., 2002; Malinow and Malenka, 2002; Sheng and Kim, 2002; Lüscher and Keller, 2004). These processes are most thoroughly understood at glutamatergic synapses, where they are mediated by postsynaptic densities (PSDs): macromolecular complexes of cell-cell adhesion proteins, scaffolding proteins, cytoskeletal proteins, regulatory enzymes, and second-messenger proteins suspended in the postsynaptic cytoplasm (Cotman et al., 1974; Banker et al., 1974; Cohen et al., 1977; see Kim and Sheng, 2004 for review). Indeed, advances in cell

Corresponding author: Alexander E. Linsalata, 330 E.Kingsley Rd. Ann Arbor, MI 48104, Phone: (631) 294-9126, latalinsa@gmail.com.

Conflict of Interest Statement: The authors report no conflict of interest.

Role of Authors: All authors had full access to all the data in the study and take responsibility for the integrity of the data and the accuracy of the data analysis. Study concept and design: AEL, TR. Acquisition of data: AEL. Analysis and interpretation of data: AEL, XC, TR. Drafting of the manuscript: AEL, TR. Critical revision of the manuscript for important intellectual content: AEL, XC, TR. Statistical analysis: AEL. Obtained funding: TR. Administrative, technical, and material support: CAW. Study supervision: TR.

fractionation, biochemistry, mass spectroscopy, electron and light microscopy, and electron tomography have converged to provide a detailed molecular understanding of glutamatergic PSDs (Sheng and Kim, 2011).

In contrast, relatively little is known about the structure and function of postsynaptic specializations at γ-aminobutyric acid (GABA)-ergic synapses, though it is known that they are composed of proteins different from those at glutamatergic PSDs (Moss and Smart, 2001). Several components of GABAergic postsynaptic specializations have been identified through their biochemical interactions with gephyrin, a 93-kDa scaffolding protein and key organizer at GABAergic and glycinergic postsynaptic sites (see Fritschy et al, 2008; Tretter et al., 2012 for review). Though originally copurified with the glycine receptor (GlyR) from rat spinal cord (Pfeiffer et al., 1982), gephyrin is widely expressed throughout the central nervous system (Triller et al., 1985; Kirsch and Betz, 1993; Mitchell et al, 1993; Cabot et al., 1995; Sassoè- Pognetto et al., 1995, 2000; Todd et al., 1995; Craig et al., 1996; Giustetto et al., 1998). The discovery that gephyrin binds to the GlyR β subunit (Meyer et al., 1995), multiple α subunits of GABA A-type receptors ($GABA_A$Rs; Tretter et al., 2008, 2011; Saiepour et al., 2010; Mukherjee et al, 2011), and polymerized tubulin (Kirsch et al., 1991) led to the hypothesis that gephyrin cross-links GlyRs and $GABA_A$Rs at postsynaptic sites to microtubules, thus stabilizing receptors opposite presynaptic sites of neurotransmitter release. This hypothesis was further developed following the discovery that isolated G and E domains of gephyrin homo-trimerize and -dimerize, respectively, in vitro, (Schwarz et al, 2001; Sola et al, 2001, 2004; Xiang et al, 2001), and that these homo-interactions are crucial for gephyrin clustering and the retention of receptors at postsynaptic sites (Calamai et al., 2005; Bedet et al., 2006; Lardi-Studler et al, 2007; Saiyed et al, 2007). These findings support the hypothesis that gephyrin forms a hexagonal scaffold at GABAergic and glycinergic postsynaptic sites that serves as a cytoplasmic platform for receptors and other intracellular binding partners (Kneussel and Betz, 2000), but such a hexagonal scaffold has yet to be directly observed.

Electron tomography has recently provided the opportunity to study the structure of synapses at nanometer resolution (Chen et al, 2008b) and has been applied successfully to characterize glutamatergic PSDs (Chen et al., 2008a, 2010; Burette et al., 2012). The purpose of the present work is to use this tool to characterize the postsynaptic specializations at GABAergic synapses. In contrast to glutamatergic PSDs, which feature a well-ordered and integral scaffold, we were surprised to find that postsynaptic specializations at GABAergic synapses feature a disordered and discontinuous network of filaments, suggesting that the machinery for capture and retention of receptors at GABAergic postsynaptic specializations is quite different from that at glutamatergic PSDs.

Materials and Methods

Antibody Characterization

Specifications for all primary antibodies used are provided in Table 1. The rabbit polyclonal antibody (pAb) against the vesicular inhibitory amino acid transporter (VIAAT), the mouse monoclonal antibody (mAb) against gephyrin, and the rabbit pAb against the $GABA_A$R α2 subunit were purchased from Synaptic Systems, and the mouse mAb against 65-kDA glutamic acid decarboxylase (GAD65) was acquired from the Developmental Studies Hybridoma Bank, University of Iowa. The anti-VIAAT pAb stains three bands of 57, 50, and 43 kDa in Western blots of purified synaptic vesicles from rat brain (manufacturer's technical information). These same three bands, which are commonly stained by other anti-VIAAT antibodies, are not present in blots of cells that do not express VIAAT (Dumoulin et al., 1999). The anti-GAD65 mAb selectively recognizes the 65-kDa isoform of GAD in blots of rat brain (Chang & Gottlieb, 1988). The anti-gephyrin mAb, clone mAb7a, has been

characterized and utilized extensively and recognizes the neuron-specific 93-kDa gephyrin isoform in blots of rat spinal cord (Pfeiffer et al., 1984). The anti-$GABA_AR$ α2 pAb stains a major band of 53 kDa in blots of purified synaptic membranes from rat brain; this band is eliminated by preadsorbtion of the antibody with its antigen peptide (manufacturer's technical information). Goat anti-rabbit and goat anti-mouse Fab' fragments conjugated to 1.4 nm-gold particles were acquired from Nanoprobes. Goat anti-rabbit and goat anti-mouse antibodies conjugated to Alexa 488 and Alexa 594, respectively, were purchased from Invitrogen.

Cultured Hippocampal Neurons

Cell culture reagents were purchased from Life Technologies except where indicated. Dissociated hippocampal neurons from Sprague-Dawley rats were cultured over glia (Lu et al., 1998) on either 22-mm glass coverslips (for immunocytochemistry) or Bal-Tec gold specimen chambers 3 mm in diameter and 300 μm deep (for high-pressure freezing/freeze-substitution). Primary glial cultures were prepared by papain digestion of hippocampi from 1 day-old rats, plated over collagen (0.16 $\mu g/mm^2$) and poly-L-lysine (MW 30- 70 kDa; 0.21 $\mu g/mm^2$) in 0.15 M sodium borate buffer (ph 8.4), and grown to confluency in 10% (v/v) fetal bovine serum in Eagle's minimum essential medium (MEM). Glial cultures were supplemented with 136 μM uridine and 54 μM 2-deoxy-5-fluoro-uridine (both from Sigma) for 1 week prior to plating of neurons. Primary neuronal cultures were prepared by trypsin digestion of hippocampi from E21 rats, plated over glial cultures, and maintained in modified MEM (Earle's salts, 33 mM glucose, 44 mM $NaHCO_3$, 5% (v/v) heat-inactivated horse serum, 1% (v/v) fetal bovine serum, 2 mM Glutamax, 136 μM uridine, 54 μM 2-deoxy-5-fluorouridine, and N3 supplement. All cultures were maintained in 10% CO_2 at 35° C. The animal protocol was approved by the NIH Animal Use and Care Committee and conformed to NIH guidelines.

Pre-embedding Immunogold Labeling

Reagents were purchased from either Sigma-Aldrich or Fischer Scientific except where indicated. DIV20-22 neuronal cultures were fixed in 4% paraformaldehyde (Electron Microscopy Sciences (EMS)) with 0.1%, 0.05%, or no glutaraldehyde (EMS) in phosphate-buffered saline (PBS), pH 7.4 for 30 (with glutaraldehyde) or 45 (without) min. They were then permeabilized and blocked with 0.1% saponin/5% normal goat serum (NGS) in PBS for 40 min, incubated with primary antibody diluted in 0.1% saponin/5% NGS in PBS for 1.5 h, incubated with gold-conjugated secondary antibody diluted in 0.1% saponin/5% NGS in PBS for 1.5 h, fixed in 2% glutaraldehyde in PBS, and silver-enhanced (HQ silver enhancement kit, Nanoprobes). Samples were processed for thin-sectioning and embedded in epoxy resins as previously described (Tao-Cheng, 2006). Immunogold labeling was absent following omission of incubation with primary antibody. Contrast, brightness, and saturation were minimally adjusted for display of electron micrographs.

Immunofluorescence and Quantitative Analysis

Three double-labeling immunocytochemistry experiments were performed in triplicate to compare labeling for VIAAT and GAD65, VIAAT and gephyrin, and $GABA_AR$α2 and gephyrin. DIV20-22 cultures were rinsed in Dulbecco's PBS, fixed with 4% paraformaldehyde/4% sucrose in 0.1 M phosphate buffer for 15 min, and permeabilized and blocked in 0.1% Triton X-100/3% NGS/2% horse serum (HS)/1% bovine serum albumin (BSA) in PBS for 30 min. They were then incubated with primary antibody diluted in 3% NGS/2% HS/1% BSA in PBS for 1 h, incubated with fluor-conjugated secondary antibody diluted in 3% NGS/2% HS/1% BSA in PBS for 1 h, and mounted on glass microscope slides in Vectashield mounting medium (Vector Laboratories). Those cultures to be incubated in pAb against $GABA_AR$α2 were first blocked in 5% HS/2% fetal bovine serum in modified

Krebs- Ringer (KR) solution (124 mM NaCl/2 mM KCl/1.24 mM KH_2PO_4/1.3 mM $MgCl_2$/2.5 mM $CaCl_2$/30 mM glucose/25 mM HEPES in dH_2O at pH 7.4) at 37°C, incubated with pAb against $GABA_AR\alpha 2$ diluted in 5% HS/2% fetal bovine serum in KR solution for 40 min at 37°C, then rinsed in KR solution before fixation. No immunofluorescence was detected when incubation with primary antibodies was omitted. Images were collected with a Zeiss LSM 510 confocal laser-scanning microscope with a 63× oil-immersion objective lens (N.A. 1.4). Contrast and brightness were minimally adjusted for display. Immunofluorescent puncta located on dendrites and cell bodies were distinguished from diffuse cytoplasmic fluorescence by intensity (≥3 SD above the mean) and size (≥0.25 m^2) threshold and were counted with Volocity Image Analysis Software (Perkin-Elmer). The percent of puncta that overlapped at least partially with puncta for the paired antibody was calculated per postsynaptic cell.

High-Pressure Freezing and Freeze-Substitution

DIV20-22 cultures on Bal-Tec gold specimen chambers were introduced to room temperature and immediately equilibrated with 0.5% ovalbumin in KR solution (osmolarity: 325), covered with hexadecane, high-pressure frozen at 2100 bar with a Bal-Tec HPM 010 freezing machine (Techno Trade), and transferred to an AFS unit (Leica Microsystems) containing 2% acrolein (EMS) in HPLC-grade acetone saturated with uranyl acetate (UA) at −160°C. Samples were brought to −90°C over 14 h, held at −90°C for 8 h, brought to −60°C over 6 h, held at −60°C for 12 h, then rinsed in acetone and methanol (Chen et al., 2008a). Samples to be processed for electron tomography were then infiltrated with Lowicryl HM20 resin in acetone following initial freeze-substitution with UA/acrolein. HM20 resin was polymerized by UV at −50°C for 2 d then vacuum-dried for 1 d. Sections 100-150 nm-thick were cut *en face* and mounted on Formvar/carbon-coated grids with fiducial markers (10 nm gold particles) affixed to both sides. In contrast, samples to be processed for thin-sectioning were instead transferred to 1% OsO_4 in acetone at −60°C for 1 h, brought to −30°C over 15 h, held at −30°C for 8 h, brought to −10°C over 4 h, acetone-rinsed and treated with 0.025% $HfCl_4$ in acetone at −10°C for 1 h, and left in acetone saturated with UA at −10°C overnight. They were subsequently brought to RT over 10 min, rinsed in acetone/methanol, embedded in epoxy resins, and sectioned identically to samples processed for immunogold labeling.

Electron Tomography

Mature GABAergic synapses in samples prepared by high-pressure freezing/freeze-substitution were identified based on their structure. Using an FEI Tecnai 300-kV electron microscope with a field-emission gun at a dose of ∼300 electrons/nm^2 per image, dual- axis tilt series were acquired at a tilt increment of 2° from −70° to +70°. Three-dimensional reconstructions were derived from these tilt series and aligned and merged using IMOD (University of Colorado), yielding tomograms comprised of 2.75 nm^3 voxels (Chen et al. 2008b), from which virtual sections 1.4 nm-thick were calculated (IMOD). Structures that extended through multiple virtual sections were analyzed in projections created by averaging consecutive virtual sections in EM3D (Stanford University). Postsynaptic membranes, membrane-associated plaques, and filaments were analyzed, segmented (manually, in at least two orthogonal cross- sectional views), and surface-rendered in Amira (Visage Imaging). Small, simple filamentous structures were analyzed first to develop a catalog of discrete structural elements, which was then used to interpret the composition of larger, more complex filamentous structures. Apparently truncated structures at the edges of tomograms were not analyzed or rendered. The length of each filament was determined using the 3D Length tool in Amira, and each filament was classified according to its length. The diameter (d) of each filament was determined by the equation $d = 2\sqrt{(A/\pi)}$, where A = the cross-sectional area of the filament in the one plane of segmentation that best approximated a plane orthogonal to the major axis of the filament. Kernel density estimation

for the lengths of filaments was calculated and plotted using optimized kernel bandwidth (Gaussian kernels, bandwidth: 0.372; Shimazaki and Shinomoto, 2012). Because the distributions of lengths and diameters of filaments were non-normal, the median absolute deviation (MAD), the median of the absolute deviations from the median of the data, have been provided for each set to summarize their variability. In addition, Mann-Whitney U tests with Bonferroni adjusted alpha levels of 0.017 (0.05/3) were applied to evaluate significant differences in length and diameter between classes of filaments.

Results

Structural Criteria for the Identification of GABAergic Synapses

Immuno-electron microscopy with antibodies against VIAAT, GAD65, and gephyrin, each one a marker of GABAergic synapses (Triller et al., 1987; Esclapez et al., 1994; Craig et al., 1996; McIntire et al, 1997; Chaudhry et al, 1998) was used to label GABAergic synapses in separate chemically-fixed samples. Criteria derived from the ultrastructure of immunolabeled synapses could then be usedto identify GABAergic synapses prepared by high-pressure freezing/freeze-substitution and select them for tomography.

Immunogold label against VIAAT and GAD65 was located almost exclusively in presynaptic boutons in close proximity to typically spherical synaptic vesicles (Fig. 1A, C). Immunogold label against gephyrin was detected predominantly along the cytoplasmic face of postsynaptic membranes, extending ∼100 nm into the cytoplasm from membranes (Fig. 1E). Distributions of label against VIAAT, GAD65, and gephyrin were consistent with previous observations (Triller et al., 1985, 1987; Dupuy & Houser, 1996; Chaudhry et al., 1998; Dumoulin et al., 1999). In most gephyrin-positive synapses, gephyrin label formed a continuous but variably concentrated band of immunogold grains along the postsynaptic membrane coextensive with synaptic vesicles abutting the presynaptic membrane. Label was typically most concentrated in the center of this band, becoming more diffuse toward its lateral margins. In gephyrin-positive synapses with bifurcated presynaptic active zones, gephyrin label was also bifurcated and located opposite synaptic vesicles at the presynaptic membrane. In some gephyrin-positive synapses, heterogeneous clustering of gephyrin label was more pronounced, leaving patches along the postsynaptic membrane without label. Microtubules, which were infrequently detected in the postsynaptic cytoplasm of axodendritic-shaft synapses, lay within ∼100 nm of and parallel to postsynaptic membranes.

VIAAT-, GAD65-, and gephyrin-positive synapses had several structural characteristics in common that distinguished them from immunonegative synapses (Fig. 1B, D, F). Relative to immunonegative synapses, immunopositive synapses typically exhibited (1) longer sites of synaptic contact (ranging 650-1400 nm in length) and (2) thinner postsynaptic accumulations of electron-dense material (∼10 nm thick), which were (3) more often discontinuous, with patches lacking electron-dense material. In addition, though immunonegative synapses were located on dendritic spines, dendritic shafts, and somas, immunopositive synapses were (4) exclusively located on dendritic shafts and somas. Immunopositive synapses seldom exhibited only three or less of these structural characteristics, and immunonegative synapses seldom exhibited one or more. Because few immunonegative synapses exhibited all four structural characteristics of immunopositive synapses, coincidence of all four characteristics at the same synapse provides substantial evidence that the synapse in question is GABAergic. We therefore derived four criteria for identifying GABAergic synapses from the structural characteristics that distinguished immunopositive synapses. Synapses satisfying all four criteria were readily identified in thin- sectioned samples prepared by high-pressure freezing/freeze-substitution (Fig. 1G, Fig. 2A, B). In addition, these putative GABAergic synapses were easily distinguished from others that resembled immunonegative synapses in chemically-fixed samples (Fig. 1H, Fig.

2C, D), suggesting that our criteria for distinguishing GABAergic synapses based on chemically-fixed samples were equally valid in samples prepared for tomography.

Double-labeling immunofluorescence confirmed that antibodies against VIAAT, GAD65, and gephyrin labeled the same population of synapses: 81.9 1.5% (mean ± SEM; n=16 cells) of immunofluorescent puncta for VIAAT located on dendrites and cell bodies overlapped at least partially with puncta for GAD65 (Fig. 3A), while 94.2 ± 1.0% (n=15 cells) of puncta for VIAAT overlapped with puncta for gephyrin (Fig. 3B). Further, the extensive overlap of immunolabeling for VIAAT and GAD65 indicated that the majority of VIAAT-positive synapses were GABAergic or mixed GABAergic/glycinergic; the rest are presumably glycinergic (Dumoulin et al, 1999; Danglot et al., 2004). Finally, double-labeling experiments with antibodies against gephyrin and $GABA_AR\alpha2$ revealed that 82.4 ± 1.8% (n=20 cells) of puncta for gephyrin overlapped with puncta for $GABA_AR\alpha2$ (Fig. 3C), confirming that the majority of GABAergic synapses were mature—gephyrin and $GABA_AR$ increasingly colocalize at synapses in vitro as they approach DIV21 (Danglot et al., 2003).

Electron Tomography Reveals a Postsynaptic Network of Filaments at GABAergic Synapses

Four complete tomographic reconstructions (ranging 74-114 nm in thickness) were derived from dual-axis tilt series of four high-pressure frozen/freeze-substituted synapses that were free of ice damage and satisfied all four structural criteria for GABAergic synapses (Fig. 4A). Analysis of 1.4 nm-thick virtual sections (Fig. 4B, Supplementary Fig. 1) calculated from reconstructions revealed diverse filamentous structures, 15.4-35.0 nm-long and 4.5-9.0 nm-wide, located in the postsynaptic cytoplasm within ∼100 nm of the postsynaptic membrane (Fig. 4D insets). While some filaments approached or contacted the postsynaptic membrane, most appeared to be suspended in the cytoplasm. Filaments that approached the membrane typically contacted irregular plaque-like structures, 12-25 nm in diameter, on the cytoplasmic face of the membrane (Fig. 4B inset). These frequently apposed smaller (5-15 nm in diameter) plaque-like structures on the synaptic-cleft face of the membrane. Some paired plaques resembled the plaques on the cytoplasmic and cleft faces of postsynaptic membranes at glutamatergic synapses, which are thought to represent transmembrane proteins with their intramembrane domains left unstained (Chen et al., 2008a, 2008b). In addition, contrary to expectations (Kirsch et al, 1991; Kirsch and Betz, 1995; Charrier et al., 2006; Hanus et al., 2006), microtubules were not present in the postsynaptic cytoplasm within ∼100 nm of postsynaptic membranes at those synapses sampled.

Projections 25.2 nm-thick (Fig. 4C) were created by averaging 18 consecutive virtual sections in series to determine the three-dimensional organization of the postsynaptic filaments, revealing that filaments contact each other and assemble into a complex network that extends ∼100 nm into the postsynaptic cytoplasm. Filaments frequently exhibited slight curves and maintained consistent diameters throughout their length. Larger, more complex filamentous structures frequently exhibited one or more dramatic kinks or changes in diameter. Since the length of stretches between kinks and sudden changes in diameter were typically consistent with the lengths of discrete filaments, these structures were interpreted as being composed of multiple interconnected filaments. In order to characterize this postsynaptic network in greater detail, filaments in two tomographic reconstructions were individually segmented in serial virtual sections and rendered (Fig. 5). Renderings of the filaments (Fig. 4D) confirmed that they indeed connect to form a postsynaptic network, though numerous filaments remain apparently unincorporated into it. Filaments and contacts between filaments were most concentrated in the center of the network within 30 nm of the postsynaptic membrane, forming a dense, partially interconnected *core* zone ∼30 nm-thick (Fig. 6). Because core zones extended beyond the confines of the section thickness, their

areas and shapes could not be known definitively. Another zone, the *periphery*, also ∼30 nm thick, encircled the core and exhibited fewer filaments and inter-filament contacts than the core. Given the more lateral location of the periphery, it might correspond to the extrasynaptic subcellular domain. In addition, a *mantle* zone, positioned between ∼30 nm and ∼100 nm deep in the postsynaptic cytoplasm and coextensive with the core and periphery zones, exhibited fewer filaments and inter-filament contacts than the core but more than the periphery. The organization of the postsynaptic network matched that of the immunogold label for gephyrin, both in distance from the postsynaptic membrane (∼100 nm) and in the increase in density of filaments and immunogold grains in the center of PSDs.

Three Classes of Filaments in the GABAergic Postsynaptic Network

The distribution of lengths of rendered postsynaptic filaments was multimodal, exhibiting two prominent peaks at 18.5 nm and 23.5 nm with three additional local maxima at 26.2 nm, 28.6 nm, and 30.5 nm (n=792 filaments; Fig. 7A). Based on this distribution, each filament was classified according to its length as either short (18.2 ± 1.2 nm (median length ± MAD), range: 15.4-21.5 nm, n=392), medium (23.2 ± 0.9 nm, range: 21.7-25.4 nm, n=287), or long (27.8 ± 1.4 nm, range: 25.7-35.0 nm, n=104) (Table 2). The diameters of short, medium, and long filaments were 6.3 ± 0.4 nm, 7.1 ± 0.4 nm, and 7.4 ± 0.5 nm (median ± MAD), respectively (Fig. 7B), and significantly different, as revealed by three independent Mann-Whitney U tests ($P<0.001$ for each comparison). Short, medium, and long filaments were located within the core, periphery, and mantle of the postsynaptic network, and no differences in the distributions of short, medium, and long filaments throughout the zones of the network were evident (Fig. 7C-E). When analyzed as independent samples, filaments at the first synapse rendered (n=487 filaments) and the second (n=305) exhibited congruent distributions of length and diameter (Fig. 8), indicating that these distributions may be shared by a significant proportion of other mature GABAergic synapses in culture.

Filaments contacted each other in three stereotyped patterns: tip-to-tip (Fig. 9A), middle- to-tip (Fig. 9B), and tip-to-tip-to-tip in an apparent trimeric configuration (Fig. 9C). Filaments of different classes exhibited mostly small, insignificant differences in their frequency of contacts (Table 2): 43 ± 2% (mean ± standard error of the mean (SEM); n=2 synapes) of filaments from the two synapses rendered contacted another filament through one of their tips; 9 ± 1% of filaments contacted other filaments through both tips; and 10 ± 1% of filaments were apparently trimerized tip-to-tip-to-tip. Short, medium, and long filaments varied, however, in frequency of middle-to-tip contacts: 9 ± 1% of short filaments, 15 ± 3% of medium filaments, and 20 ± 2% of long filaments contacted another filament middle-to-tip. Pearson's chi-squared test of independence revealed a significant relationship between filament class and frequency of middle-to-tip contacts ($P<0.05$, n=792), with short filaments less likely and long filaments more likely to form contacts. In total, 58 ± 1% of short filaments, 58 ± 3% of medium filaments, and 55 ± 4% of long filaments contacted other filaments.

The GABAergic Post-Synaptic Network is a Conglomerate of Multi-Filament Complexes

Postsynaptic filaments, interconnected through tip-to-tip, middle-to-tip, and tip-to-tip-to-tip modes of contact, formed complexes composed of 2-12 filaments each (Fig. 9D). Unconnected filaments, two-filament complexes, and three-filament complexes were predominant, accounting for 67 ± 1% (mean ± SEM, n=2 synapses), 17 ± 1%, and 8 ± 1%, respectively, of mono- and poly-filament structures in the postsynaptic networks (Fig. 9E). Indeed, 41 ± 1% (mean ± SEM, n=2) of filaments contacted no other filaments, while 22 ± 1% and 13 ± 2% of filaments were incorporated into two- and three-filament complexes, respectively, indicating that the majority of postsynaptic filaments at GABAergic synapses

were not incorporated into an integrated scaffold. Unconnected filaments, two-filament complexes, and three-filament complexes were distributed throughout the postsynaptic network, while four- to twelve-filament complexes tended to cluster within the core, though complexes composed of more than three filaments were occasionally located in the periphery and mantle (Fig. 9F-H). In the core, unconnected filaments, two-filament complexes, and three-filament complexes were intercalated between the four- to twelve-filament complexes.

Complexes were occasionally contacted by irregular globules of electron-dense material. To determine whether separate complexes were inter-linked through this material, those globules that contacted multiple complexes were rendered. A minority of complexes throughout the postsynaptic network were, in fact, inter-linked through these globules, forming multiple clutches of interconnected complexes composed of 2-15 filaments each (Fig 9I). The largest clutches were located in the core of the network and were surrounded by smaller clutches, smaller complexes, and unconnected filaments in the periphery and mantle. Most complexes, however, were not linked through electron-dense globules, and therefore the organization of the postsynaptic network was not significantly revised by the inclusion of this additional material. The postsynaptic network at GABAergic synapses thus resembles a loose conglomerate of disconnected mono- and poly-filament structures, with the largest of these structures positioned toward its center within 30 nm of the postsynaptic membrane.

Discussion

Electron tomography was used to examine the molecular organization of GABAergic postsynaptic specializations in hippocampal cultures. Criteria for the selection of GABAergic synapses for tomography were derived from the structure of GABAergic synapses identified by immunogold labeling. The validity of the criteria is supported by the similarities between the structure of these immunolabeled synapses and the previously documented structure of inhibitory synapses: type II synapses (Gray, 1959) and symmetrical synapses (Colonnier, 1968) in the cerebral cortex, as well as synapses with analogous structure in the hippocampus, cerebellum, spinal cord, and retina (McLaughlin et al., 1975a, 1975b; Raviola & Raviola, 1967; Kosaka et al., 1984). GABAergic synapses selected for tomography were likely to be structurally mature, as shown by the convergence of labeling for essential synaptic proteins by 20-22 days in culture (Craig et al., 1996; Danglot et al., 2003; Kuriu et al., 2012).

Analysis of the tomographic renderings revealed a postsynaptic network at GABAergic synapses that is composed of at least three classes of filaments distinguished by significant differences in length and diameter. Because the different classes of filaments exhibited coincident distributions throughout the network, as well as similar frequencies and modes of contact with other filaments and plaques on the postsynaptic membrane, the filaments may well be composed of the same or similar proteins. Moreover, the correspondence between the organization of the postsynaptic networks and the distribution of gephyrin immunogold-labeling implies that gephyrin is distributed throughout the network.

Cytoplasmic structures in tomograms can be identified by comparing their dimensions to those of purified molecules (Chen et al., 2008a, 2008b), but information about the dimensions of the gephyrin molecule is limited as only the distal G and E domains of gephyrin have been crystallized (Schwarz et al., 2001; Sola et al., 2001, 2004; Xiang et al., 2001). Because the central C domain, which bridges the G and E domains, has not been characterized, the full length of the gephyrin molecule and the exact spatial relation of the G and E domains to each other can only be estimated. It is possible to arrange G and E

domains and homo-G and homo-E dimers into theoretical structures that both agree with the reported oligomerization properties of gephyrin and approximate the dimensions of short, medium, and long filaments (Linsalata et al., 2011). Each of these structures would be predicted to have unique patterns of binding with other gephyrin molecules, but short, medium, and long filaments do not exhibit the patterns of contact with other filaments predicted by this interpretation. Short, medium, and long filaments could instead represent different splice variants of gephyrin, as multiple variants are expressed in the brain and spinal cord (Prior et al., 1992; Meier et al., 2000). These variants differ in affinity for the GlyR β subunit, stability of folding, sites of phosphorylation, and postsynaptic clustering (Meier et al, 2000; Bedet et al, 2006; Lardi-Studler et al., 2007; Herweg and Schwarz, 2012), but it is unclear how variants differ in size. While the GABAergic postsynaptic network is likely to include a large number of gephyrin molecules, whether and how these correspond to the classes of postsynaptic filaments remains unclear.

Because the distal G and E domains of gephyrin are able to homo-trimerize and - dimerize, respectively (Schwarz et al., 2001; Sola et al., 2001, 2004; Xiang et al., 2001), gephyrin has been proposed to form a hexagonal lattice in the cytoplasm beneath the postsynaptic membrane (Xiang et al., 2001; Sola et al., 2004) that limits the lateral diffusion of $GABA_A$Rs and GlyRs at postsynaptic sites (Meier et al., 2001; Dahan et al., 2003; Jacob et al., 2005). Indeed, several splice variants and mutants of gephyrin with reduced capacity to homo- trimerize and -dimerize through G- and E-domain interactions also exhibited reduced clustering and retention of $GABA_A$Rs and GlyRs at postsynaptic sites (Bedet et al., 2006; Lardi-Studler et al, 2007; Saiyed et al., 2007; Calamai et al., 2009). Nevertheless, we were unable to detect any indication of a hexagonal lattice in detailed tomographic renderings of the postsynaptic network at GABAergic synapses.

The structure of the postsynaptic network provides several hints as to its function. The denser, partially interconnected core of the network is surrounded by the less dense and less interconnected periphery and mantle, leading us to speculate that filaments of the periphery and mantle might become integrated into the core in response to particular physiological stimuli. In addition, core filaments frequently contacted plaques on the cytoplasmic face of the postsynaptic membrane. Some cytoplasmic-face plaques appeared to be paired with apposing cleft-face plaques. At glutamatergic synapses paired plaques are thought to correspond to αBamino-3- hydroxy-5-methyl-4-isoxazolepropionic acid (AMPA) and N-methyl-D-aspartate (NMDA) receptors (Chen et al., 2008a, 2008b). Fluorescent labeling indicates that $GABA_A$Rs are present at GABAergic synapses by 20-22 days in culture (Craig et al., 1996; Danglot et al., 2003), so the paired plaques on postsynaptic membranes might well represent $GABA_A$Rs. The postsynaptic network might therefore play a key role in the capture and retention of membrane-associated proteins such as $GABA_A$Rs, GlyRs (Danglot et al., 2004), or K^+-channels (Du et al., 1998).

Electron tomography revealed a surprising feature of GABAergic postsynaptic networks that distinguishes them from glutamatergic PSDs. While scaffolding elements at glutamatergic PSDs generally contact each other in regular patterns to form a continuous structure (Chen et al., 2008a), filaments of GABAergic postsynaptic networks form irregular complexes that are infrequently linked through globules of electron-dense material. Indeed, this contrast between glutamatergic PSDs and GABAergic postsynaptic specializations is more striking than what traditional electron microscopy has so far revealed. If these filaments do not form an integrated, continuous scaffold, how does the postsynaptic network maintain its integrity and regulate the distribution of intramembrane and cytoplasmic components?

We propose that the filaments of the GABAergic postsynaptic network may be held together through weak, transient connections that do not impose a rigid pattern on the network.

Filaments might rapidly establish, break, and re-establish connections with other filaments around them such that filaments remain part of the network through their numerous but transient interactions with other filaments. The transience of filament interactions would explain the apparent splitting and merging behaviors of postsynaptic gephyrin clusters apposed to the same GABAergic bouton (Dobie and Craig, 2012; Kuriu et al., 2012): failure to re-establish connections between filaments could lead to the fragmentation of the postsynaptic network, after which the resulting fragments diffuse apart. In addition, if coupled with mechanisms that modulate the strength and stability of inter-filament connections, a highly labile postsynaptic network would allow the capture and retention of $GABA_A$Rs at postsynaptic sites to be continuously regulated. These findings illustrate that receptors at GABAergic postsynaptic sites might be maintained and regulated through strategies that are distinct from those at glutamatergic synapses.

Supplementary Material

Refer to Web version on PubMed Central for supplementary material.

Acknowledgments

We thank Virginia Crocker and Rita Azzam of the NINDS electron-microscopy facility for technical support in electron microscopy, Carolyn Smith of NINDS for help in analyzing the immunofluorescence experiments, and Alioscka Sousa of NIBIB for help in collecting tilt series. The GAD-6 monoclonal antibody developed by David I. Gottlieb (Washington University School of Medicine, St. Louis, MO) was obtained from the Developmental Studies Hybridoma Bank developed under the auspices of the National Institute of Child Health and Human Development and maintained by the University of Iowa, Department of Biological Sciences, Iowa City, IA 52242.

Support: Intramural Program, NINDS/NIH

Literature Cited

Balice-Gordon RJ, Lichtman JW. In vivo observations of pre- and postsynaptic changes during the transition from multiple to single innervation at developing neuromuscular junctions. J Neurosci. 1993; 13(2):834–855. [PubMed: 8426240]

Banker G, Churchill L, Cotman CW. Proteins of the postsynaptic density. J Cell Biol. 1974; 63:456–465. [PubMed: 4419608]

Bedet C, Bruusgaard JC, Vergo S, Groth-Pedersen L, Eimer S, Triller A, Vannier C. Regulation of gephyrin assembly and glycine receptor synaptic stability. J Biol Chem. 2006; 281(4):30046–30056. [PubMed: 16882665]

Burette AC, Lesperance T, Crum J, Martone M, Volkmann N, Ellisman MH, Weinberg RJ. Electron tomographic analysis of synaptic ultrastructure. J Comp Neurol. 2012; 520:2697–2711. [PubMed: 22684938]

Cabot JB, Bushnell A, Alessi V, Mendell NR. Postsynaptic gephyrin immunoreactivity exhibits a nearly one-to-one correspondence with gamma-aminobutyric acid-like immunogold- labeled synaptic inputs to sympathetic preganglionic neurons. J Comp Neurol. 1995; 356:418–432. [PubMed: 7642803]

Calamai M, Spect CG, Heller J, Alcor D, Machado P, Vannier C, Triller A. Gephyrin oligomerization controls GlyR mobility and synaptic clustering. J Neurosci. 2009; 29(24):7639–7648. [PubMed: 19535575]

Charrier C, Ehrensperger MV, Dahan M, Lévi S, Triller A. Cytoskeleton regulation of glycine receptor number at synapses and diffusion in the plasma membrane. J Neurosci. 2006; 26(33):8502–8511. [PubMed: 16914675]

Chaudry FA, Reimer RJ, Bellocchio EE, Danbolt NC, Osen KK, Edwards RH, Storm-Mathisen J. The vesicular GABA transporter, VGAT, localizes to synaptic vesicles in sets of glycinergic as well as GABAergic neurons. J Neurosci. 1998; 18(23):9733–9750. [PubMed: 9822734]

Chen X, Nelson CD, Li X, Winters CA, Azzam R, Sousa AA, Leapman RD, Gainer H, Sheng M, Reese TS. PSD-95 is required to sustain the molecular organization of the postsynaptic density. J Neurosci. 2011; 31(17):6329–6338. [PubMed: 21525273]

Chen X, Winters CA, Azzam R, Li X, Galbraith JA, Leapman RD, Reese TS. Organization of the core structure of the postsynaptic density. PNAS. 2008a; 105(11):4453–4458. [PubMed: 18326622]

Chen X, Winters CA, Reese TS. Life inside a thin section: tomography. J Neurosci. 2008b; 28(38): 9321–9327. [PubMed: 18799665]

Cotman CW, Banker G, Churchilll L, Taylor D. Isolation of postsynaptic densities from rat brain. J Cell Biol. 1974; 63:441–455. [PubMed: 4138148]

Cohen RS, Blomberg F, Berzins F, Siekevitz P. The structure of postsynaptic densities isolated from dog cerebral cortex. J Cell Biol. 1977; 74:181–203. [PubMed: 194906]

Colonnier M. Synaptic patterns on different cell types in the different laminae of the cat visual cortex: an electron microscope study. Brain Res. 1968; 9:268–287. [PubMed: 4175993]

Craig AM, Banker G, Chang W, McGrath ME, Serpinskaya AS. Clustering of gephyrin at GABAergic but non glutamatergic synapses in cultured rat hippocampal neurons. J Neurosci. 1996; 16(10): 3166–3177. [PubMed: 8627355]

Dahan M, Lévi S, Luccardini C, Rostaing P, Riveau B, Triller A. Diffusion dynamics of glycine receptors revealed by single-quantum dot tracking. Science. 2003; 302:442–445. [PubMed: 14564008]

Danglot L, Rostaing P, Triller A, Bessis, A. Morphologically identified glycinergic synapses in the hippocampus. Mol Cell Neurosci. 2004; 27:394–403. [PubMed: 15555918]

Danglot L, Triller A, Bessis A. Association of gephyrin with synaptic and extrasynaptic $GABA_A$ receptors varies during development in cultured hippocampal neurons. Mol Cell Neurosci. 2003; 23:264–278. [PubMed: 12812758]

Dobie FA, Craig AM. Inhibitory synapse dynamics: coordinated presynaptic and postsynaptic mobility and the major contribution of recycled vesicles to new synapse formation. J Neurosci. 2011; 31(29):10481–93. [PubMed: 21775594]

Du J, Tao-Cheng JH, Zerfas P, McBain CJ. The K^+ channel, $K_V2.1$, is apposed to astrocytic processes and is associated with inhibitory postsynaptic membranes in hippocampal and cortical principal neurons and inhibitory interneurons. Neuroscience. 1998; 84(1):37–48. [PubMed: 9522360]

Dumoulin A, Rostaing P, Bedet C, Levi S, Isambert MF, Henry JP, Triller A, Gasnier B. Presence of the vesicular inhibitory amino acid transporter in GABAergic and glycinergic synaptic terminal boutons. J Cell Science. 1999; 112:811–823. [PubMed: 10036231]

Dupuy ST, Houser CR. Prominent expression of two forms of glutamate decarboxylase in the embryonic and early postnatal rat hippocampal formation. J Neurosci. 1996; 16(21):6919–6932. [PubMed: 8824330]

Esclapez M, Tillakaratne NJK, Kaufman DL, Tobin AJ, Houser CR. Comparative localization of two forms of glutamic acid decarboxylase and their mRNAs in rat brain supports the concept of functional differences between the forms. J Neurosci. 1994; 14(3):1834–1855. [PubMed: 8126575]

Fritschy JM, Harvey RJ, Schwarz, G. Gephyrin: where do we stand, where do we go? Trends Neurosci. 2008; 31(5):257–264. [PubMed: 18403029]

Gaiarsa JL, Caillard O, Ben-Ari Y. Long-term plasticity at GABAergic and glycinergic synapses: mechanisms and functional significance. Trends Neurosci. 2002; 25(11):564–570. [PubMed: 12392931]

Giustetto M, Kirsch J, Fritschy JM, Cantino D, Sassoè-Pognetto M. Localization of the clustering protein gephyrin at GABAergic synapses in the main olfactory bulb of the rat. J Comp Neurol. 1998; 395:231–244. [PubMed: 9603375]

Gray EG. Axo-somatic and axo-dendritic synaptses of the cerebral cortex: an electron microscope study. J Anat. 1959; 93:420–33. [PubMed: 13829103]

Hanus C, Ehrensperger MV, Triller A. Activity-dependent movements of postsynaptic scaffolds at inhibitory synapses. J Neurosci. 2006; 26(17):4586–4595. [PubMed: 16641238]

Herweg J, Schwarz G. Splice-specific glycine receptor binding, folding, and phosphorylation of the scaffolding protein gephyrin. J Biol Chem. 2012; 287(16):12645–12656. [PubMed: 22351777]

Kneussel M, Betz H. Clustering of inhibitory neurotransmitter receptors at postsynaptic sites: the membrane activation model. Trends Neurosci. 2000; 23(9):429–435. [PubMed: 10941193]

Kim E, Sheng M. PDZ domain proteins of synapses. Nat Rev Neurosci. 2004; 5:771–781. [PubMed: 15378037]

Kirsch J, Betz H. Widespread expression of gephyrin, a putative glycine receptor-tubulin linker protein, in rat brain. Brain Res. 1993; 621:301–310. [PubMed: 8242343]

Kirsch J, Betz H. The postsynaptic localization of the glycine receptor-associated protein gephyrin is regulated by the cytoskeleton. J Neurosci. 1995; 15(6):4148–4156. [PubMed: 7790902]

Kirsch J, Langosch D, Prior P, Littauer UZ, Schmitt B, Betz H. The 93-kDA glycine receptor-associated protein binds to tubulin. J Biol Chem. 1991; 266(33):22242–22245. [PubMed: 1657993]

Kosaka T, Hama K, Wu JY. GABAergic synaptic boutons in the granule cell layer of rate dentate gyrus. Brain Res. 1984; 293:353–359. [PubMed: 6320972]

Kuriu T, Yanagawa Y, Konishi S. Activity-dependent coordinated mobility of hippocampal inhibitory synapses visualized with presynaptic and postsynaptic tagged-molecular makers. Mol Cell Neurosci. 2012; 49:184–195. [PubMed: 22146684]

Jacob TC, Bogdanov YD, Magnus C, Saliba RS, Kittler JT, Haydon PG, Moss SJ. Gephyrin regulates the cell surface dynamics of synaptic $GABA_A$ receptors. J Neurosci. 2005; 25(45):10469–10478. [PubMed: 16280585]

Lardi-Studler B, Smolinksy B, Petitjean CM, Koenig F, Sidler C, Meier JC, Fritschy JM, Schwarz G. Vertebrate-specific sequences in the gephyrin E-domain regulate cytosolic aggregation and postsynaptic clustering. J Cell Science. 2007; 120:1271–1282.

Linsalata, AE.; Chen, X.; Winters, CA.; Reese, TS. Electron tomography of the GABAergic PSD in dissociated hippocampal cultures. Poster presented at: Neuroscience 2011 41st Annual Meeting of the Society for Neuroscience; 2011 November; Washington, D.C. USA. 2011.

Lu Z, McLaren RS, Winters CA, Ralston E. Ribosome association contributes to restricting mRNAs to the cell body of hippocamapal neurons. Mol Cell Neurosci. 1998; 12:363–375. [PubMed: 9888989]

Lüscher B, Keller CA. Regulation of $GABA_A$ receptor trafficking, channel activity, and functional plasticity of inhibitory synapses. Pharmacology & Therapeutics. 2004; 102:195–221. [PubMed: 15246246]

Malinow R, Malenka RC. AMPA receptor trafficking and synaptic plasticity. Annu Rev Neurosci. 2002; 25:103–126. [PubMed: 12052905]

Meyer G, Kirsch J, Betz H, Langosch D. Identification of a gephyrin binding motif on the glycine receptor β subunit. Neuron. 1995; 15:563–572. [PubMed: 7546736]

McIntire SL, Reimer RJ, Schuske K, Edwards RH, Jorgensen EM. Identification and characterization of the vesicular GABA transporter. Letters to Nat. 1997; 389:870–876.

McLaughlin BJ, Barber R, Saito K, Roberts E, Wu JY. Immunocytochemical localization of glutamate decarboxylase in rat spinal cord. J Comp Neurol. 1975a; 164:305–322. [PubMed: 1184786]

McLaughlin BJ, Wood JG, Saito K, Roberts E, Wu JY. The fine structural localization of glutamate decarboxylase in developing axonal processes and presynaptic terminals of rodent cerebellum. Brain Res. 1975b; 85:355–371. [PubMed: 1089460]

Meier J, De Chaldée M, Triller A, Vannier C. Functional heterogeneity of gephyrins. Mol Cell Neurosci. 2000; 16:566–577. [PubMed: 11083919]

Meier J, Vannier C, Sergé A, Triller A, Choquet D. Fast and reversible trapping of surface glycine receptors by gephyrin. Nat Neurosci. 2001; 4(3):253–260. [PubMed: 11224541]

Mitchell K, Spike RC, Todd AJ. An immunocytochemical study of glycine and GABA in laminae I-III of rat spinal dorsal horn. J Neurosci. 1993; 13(6):2371–2381. [PubMed: 8388921]

Moss SJ, Smart TG. Constructing inhibitory synapses. Nat Rev Neurosci. 2001; 2(4):240–250. [PubMed: 11283747]

Mukherjee J, Kretschmannova K, Gouzer G, Maric HM, Ramsden S, Tretter V, Harvey K, Davies PA, Triller A, Schindelin H, Moss SJ. The residence time of GABA(A)Rs at inhibitory synapses is determined by direct binding of the receptor α1 subunit to gephyrin. J Neurosci. 2011; 31(41): 14677–14687. [PubMed: 21994384]

Pfeiffer F, Graham D, Betz H. Purification by affinity chromatography of the glycine receptor of rat spinal cord. J Biol Chem. 1982; 257(16):9389–9393. [PubMed: 6286620]

Prior P, Schmitt B, Grenningloh G, Pribilla I, Multhaup G, Beyreuther K, Maulet Y, Werner P, Langosch D, Kirsch J, Betz H. Primary structure and alternative splice variants of gephyrin, a putative glycine receptor-tubulin linker protein. Neuron. 1992; 8:1161–1170. [PubMed: 1319186]

Raviola G, Raviola E. Light and electron microscopic observations on the inner plexiform layer of the rabbit retina. Am J Anat. 1967; 120:402–426.

Saiepour L, Fuchs C, Patrizi A, Sassoè-Pognetto M, Harvey RJ, Harvey M. Complex role of collybistin and gephyrin in $GABA_A$ receptor clustering. J Biol Chem. 2010; 285:29623–31. [PubMed: 20622020]

Saiyed T, Paarman I, Schmitt B, Haeger S, Sola M, Schmalzig G, Weissenhorn W, Betz H. Molecular basis of gephyrin clustering at inhibitory synapses. J Biol Chem. 2007; 282(38):5625–5632. [PubMed: 17182610]

Sassoè-Pognetto M, Kirsch J, Grünert U, Greferath U, Fritschy JM, Möhler H, Betz H, Wässle H. Colocalization of gephyrin and $GABA_A$-receptor subunits in the rat retina. J Comp Neurol. 1995; 357:1–14. [PubMed: 7673460]

Sassoè-Pognetto M, Panzanelli P, Sieghart W, Fritschy JM. Colocalization of multiple $GABA_A$ receptor subtypes with gephyrin at postsynaptic sites. J Comp Neurol. 2000; 420:481–498. [PubMed: 10805922]

Schwarz G, Schrader N, Mendel RR, Hecht HJ, Schindelin H. Crystal structures of human gephyrin and plant Cnx1 G domains: comparative analysis and functional implications. J Mol Biol. 2001; 312(2):405–418. [PubMed: 11554796]

Sheng M, Kim E. The postsynaptic organization of synapses. Cold Spring Harb Perspect Biol. 2011; 3:a005678. [PubMed: 22046028]

Sheng M, Kim MJ. Postsynaptic signaling and plasticity mechanisms. Science. 2002; 298:776–780. [PubMed: 12399578]

Shimazaki H, Shinomoto S. Kernel bandwidth optimization in spike rate estimation. J Comput Neurosci. 2010; 29:171–182. [PubMed: 19655238]

Sola M, Bavro VN, Timmins J, Franz T, Ricard-Blum S, Schoehn G, Ruigrok RWH, Paarmann I, Saiyed T, O'Sullivan GA, Schmitt B, Betz H, Weissenhorn W. Structural basis of dynamic glycine receptor clustering by gephyrin. EMBO J. 2004; 23:2510–2519. [PubMed: 15201864]

Sola M, Kneussel M, Heck IS, Betz H, Weissenhorn W. X-ray crystal structure of the trimeric N-terminal domain of gephyrin. J Biol Chem. 2001; 276(27):25294–25301. [PubMed: 11325967]

Somogyi P, Halasy K, Somogyi J, Storm-Mathiesen J, Ottersen OP. Quantification of immunogold labeling reveals enrichment of glutamate in mossy and parallel fibre terminals in cat cerebellum. Neuroscience. 1986; 19:1045–1050. [PubMed: 2881226]

Tao-Cheng JH. Activity-related redistribution of presynaptic proteins at the active zone. Neuroscience. 2006; 141:1217–1224. [PubMed: 16757121]

Todd AJ, Spike RC, Chong D, Neilson M. The relationship between glycine and gephyrin in synapses of the rat spinal cord. Euro J Neurosci. 1995; 7:1–11.

Tretter V, Jacob TC, Mukherjee J, Fritschy JM, Pangalos MN, Moss SJ. The clustering of $GABA_A$ receptor subtypes at inhibitory synapses is facilitated via the direct binding of receptor $\alpha 2$ subunits to gephyrin. J Neurosci. 2008; 28(6):1356–1365. [PubMed: 18256255]

Tretter V, Kerschner B, Milenkovic I, Ramsden SL, Ramerstorfer J, Saiepour L, Maric HM, Moss SJ, Schindelin H, Harvey RJ, Sieghart W, Harvey K. Molecular basis of the γ- aminobutyric acid A receptor $\alpha 3$ subunit interaction with the clustering protein gephyrin. J Biol Chem. 2011; 286(43): 37702–37711. [PubMed: 21880742]

Tretter V, Mukherjee J, Maric HM, Schindlein H, Sieghart W, Moss SJ. 2012. Gephyrin, the enigmatic organizer at GABAergic synapses. Frontiers Cell Neurosci. 2012; 6:1–16.

Triller A, Cluzeaud F, Korn H. Gamma-aminobutyric acid-containing terminals can be apposed to glycine receptors at central synapses. J Cell Biol. 1987; 104:947–956. [PubMed: 3031086]

Triller A, Cluzeaud F, Pfeiffer F, Betz H, Korn H. Distribution of glycine receptors at central synapses: an immunoelectron microscopy study. J Cell Biol. 1985; 101:683–688. [PubMed: 2991304]

Xiang S, Nichols J, Rajagopalan KV, Schindelin H. The crystal structure of Escherichia coli MoeA and its relationship to the multifunctional protein gephyrin. Structure. 2001; 9:299–310. [PubMed: 11525167]

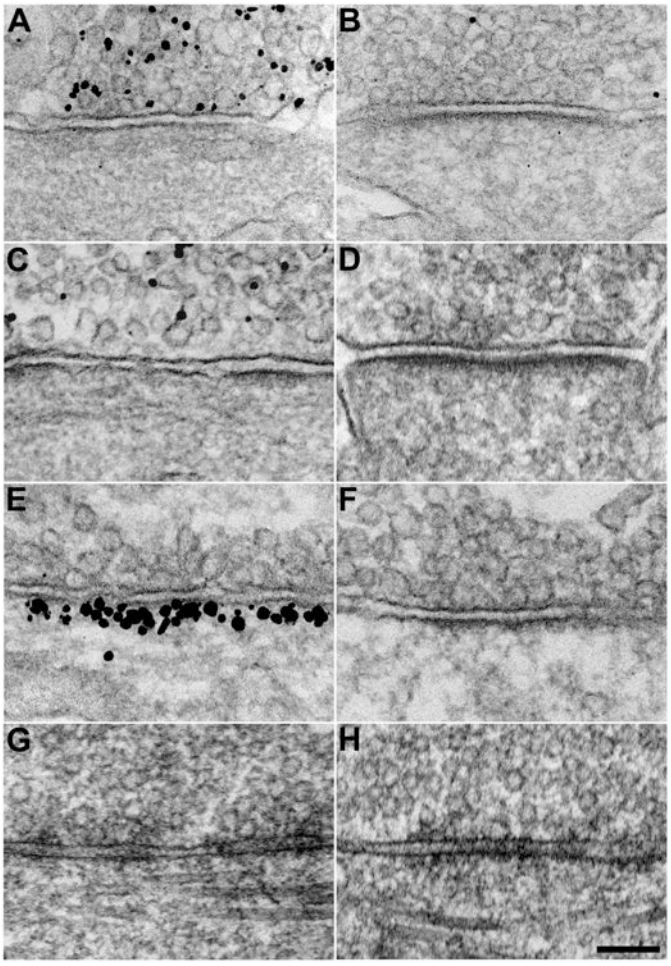

Figure 1. Ultrastructural characterization of GABAergic synapses identified by immunocytochemistry

A, B, Representative electron micrographs of synapses prepared by chemical fixation that exhibit (A) and do not exhibit (B) immunogold labeling for vesicular inhibitory amino acid transporter (VIAAT). **C, D,** Synapses that exhibit (C) and do not exhibit (D) immunogold labeling for 65-kDA glutamic acid decarboxylase (GAD65). **E, F,** Synapses that exhibit (E) and do not exhibit (F) immunogold labeling for gephyrin. VIAAT-positive, GAD65-positive, and gephyrin-positive synapses typically exhibit patchy, discontinuous PSDs that are thinner and longer than PSDs at unlabeled synapses. In addition, VIAAT-positive, GAD65-positive, and gephyrin-positive synapses are located exclusively on cell bodies and dendritic shafts, whereas unlabeled synapses are located on spines as well. **G, H,** Representative electron micrographs of synapses prepared by high-pressure freezing/freeze-substitution that share structural characteristics with VIAAT-positive, GAD65-positive, and gephyrin-positive synapses (G) or with unlabeled synapses (H) (Scale bar: 100 nm.)

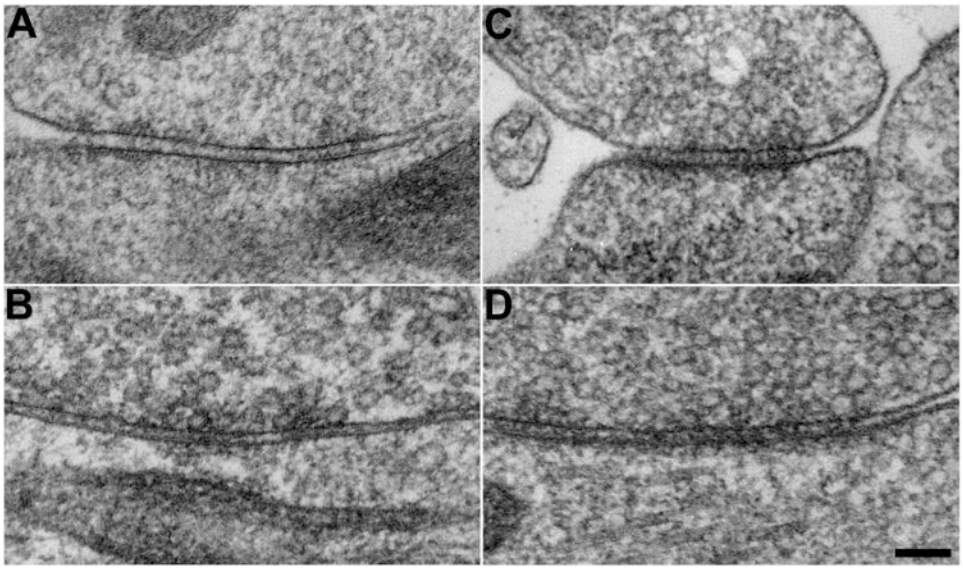

Figure 2. High-pressure frozen/freeze-substituted GABAergic synapses are distinguished by their ultrastructural characteristics

A-D, Representative electron micrographs of putative GABAergic synapses (A, B) and non-GABAergic synapses (C, D) prepared by high-pressure freezing/freeze-substitution. The distinguishing ultrastructural characteristics of GABAergic synapses remain apparent after freeze-substitution. (Scale bar: 100 nm.)

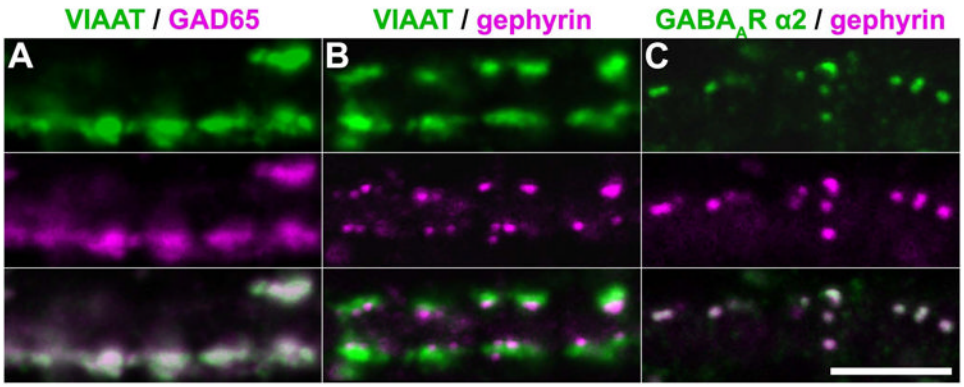

Figure 3. Convergence of immunofluorescence against VIAAT, GAD65, gephyrin, and the GABA$_A$ receptor α2 subunit on dendrites

A-C, Representative confocal sections ~1 um-thick showing the overlap of immunofluorescent puncta for VIAAT (green) and GAD65 (magenta) (A), VIAAT (green) and gephyrin (magenta) (B), and the GABA$_A$ receptor α2 subunit (green) and gephyrin (magenta) (C) on dendrites. Extensive overlap of puncta for VIAAT, GAD65, and gephyrin indicates that these antibodies label the same population of synapses in DIV20-22 dissociated hippocampal cultures. In addition, the overlap of puncta for GABA$_A$ receptor α2 and gephyrin suggests that GABAergic synapses were predominantly mature by this point. (Scale bar: 5 μm.)

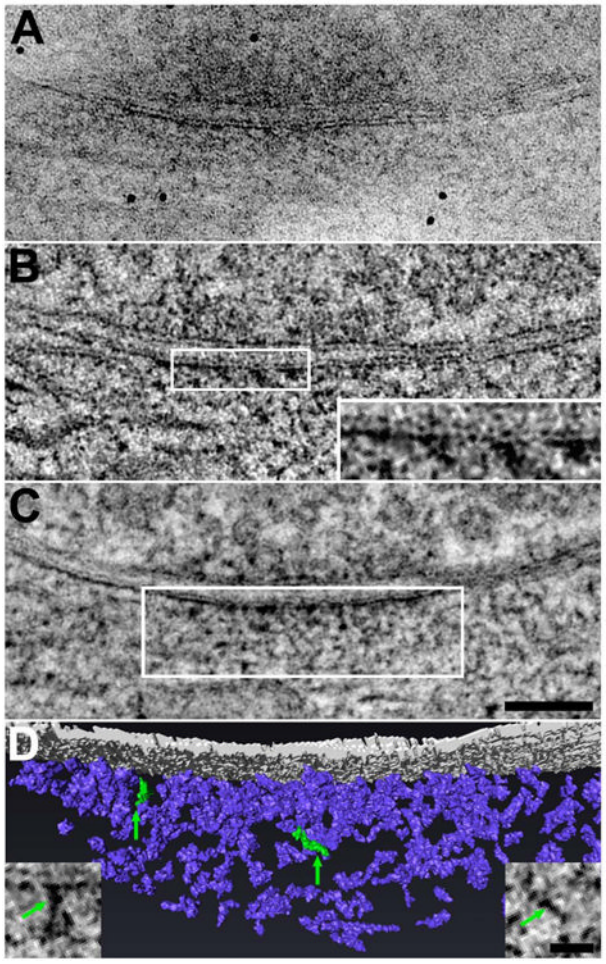

Figure 4. Electron tomography of GABAergic synapses reveals a postsynaptic network of filaments

A, Electron micrograph of an axodendritic-shaft synapse identified as GABAergic by its structure after preparation by high-pressure freezing/freeze-substitution. Details in the PSD are partially obscured by overlap in this 125 nm-thick section. **B**, Filament-like structures lining the cytoplasmic face of the post-synaptic membrane become evident in 1.4 nm-thick virtual sections derived from the tomogram of the synapse depicted in A. Plaque-like structures on both faces of the postsynaptic membrane are also evident (inset; magnification doubled). **C,** A 25 nm-thick projection derived from 18 superimposed virtual sections (and centered around the virtual section presented in B) suggests that the postsynaptic filaments form an intricate network extending ∼100 nm into the cytoplasm. (Scale bar: 100 nm.) **D,** Rendering of the postsynaptic filaments (postsynaptic membrane rendered in gray, filaments in violet). The rendering depicts the boxed field in C. Insets are virtual sections showing representative filaments, highlighted in green in the rendering. (Scale bar: 25 nm.)

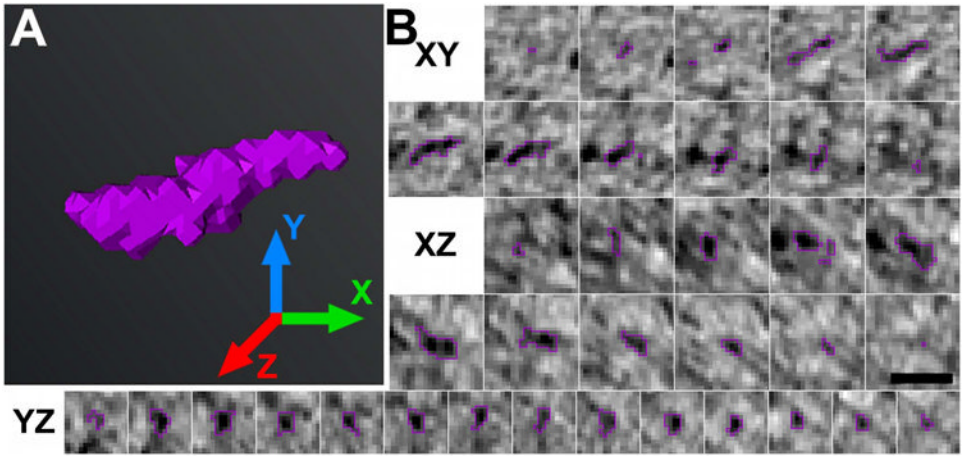

Figure 5. Segmentation in multiple orthogonal views enables accurate three-dimensional analysis of each postsynaptic filament

A, Rendering of a discrete postsynaptic filament (violet) with X, Y, and Z axes indicated. **B,** Series of consecutive cross sections in the XY, XZ, and YZ views of the filament rendered in A. Cross sections were cropped from virtual sections 1.4 nm-thick, which were calculated from the tomographic reconstruction. The filament is outlined in violet for clarity. Segmentation in multiple planes permitted a more exact description of filaments' size, shape, and relation to other structures. (Scale bar: 20 nm.)

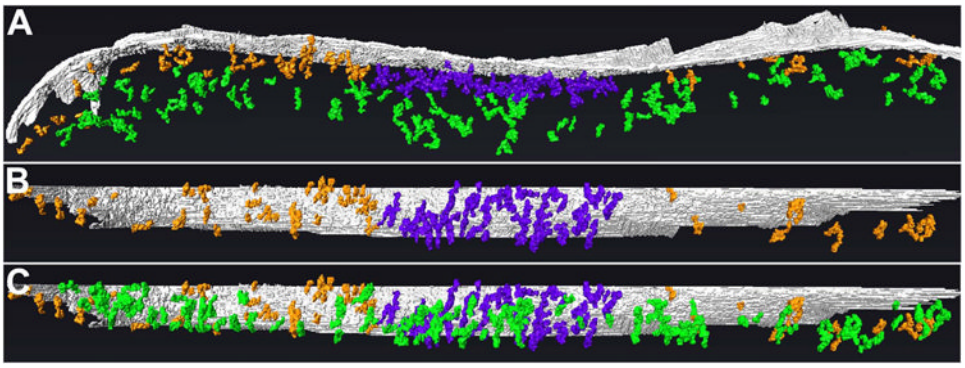

Figure 6. The postsynaptic network of filaments at GABAergic synapses consists of distinct zones

A, Rendering (side-view) of the *core*, *periphery*, and *mantle* of the postsynaptic network. The *core* (rendered in violet), extending ∼30 nm into the cytoplasm from the postsynaptic membrane (gray), exhibits the greatest concentration of filaments and contacts between filaments. The *periphery* (orange), which appears to encircle the core, also extends ∼30 nm into the cytoplasm but exhibits a low concentration of filaments and inter-filament contacts. The *mantle* (green), located between ∼30 and ∼100 nm from the postsynaptic membrane and co- extensive with the core and periphery, exhibits fewer filaments and inter-filament connections than the core but more than the periphery. **B**, *En-face* view of postsynaptic membrane and network, omitting filaments of the mantle to visualize without obstruction the division between the core and periphery. **C**, *En-face* view of postsynaptic membrane and network, showing extent of the mantle.

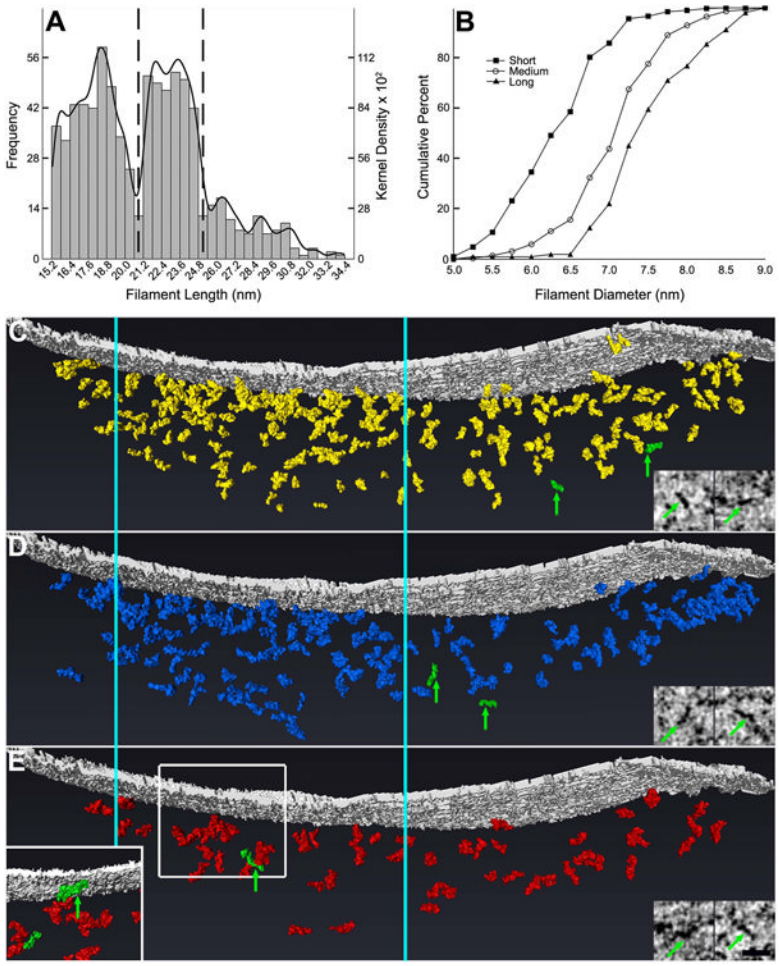

Figure 7. At least three classes of filaments contribute to the postsynaptic network at GABAergic synapses

A, Frequency histogram of the lengths of rendered filaments with kernel density estimation. Histogram bars correspond to left y axis; kernel density estimation curve corresponds to right y axis. Local minima at 20.7 nm and 25.5 nm suggest that there are three distinct classes of filaments within postsynaptic networks of GABAergic synapses. Filaments were classified as *short*, *medium*, or *long* based on their lengths: dotted vertical lines illustrate the divisions between classes of filaments. **B,** Cumulative frequency curves for the diameters of short, medium, and long filaments illustrating significant differences between diameters of filament classes, with short filaments exhibiting the smallest diameters and long filaments exhibiting the largest. There is considerable overlap between classes, however. **C-E,** Short (C; rendered in yellow), medium (D; blue), and long filaments (E; red) are similarly distributed throughout the GABAergic postsynaptic network, with filaments most highly concentrated at the core (located between the vertical cyan lines that extend through C, D, and E) and least concentrated in the periphery. Representative filaments of each class are highlighted in green in the rendering and correspond to the filaments in the adjoining virtual sections. The inset in E depicts the boxed field rotated 180° about the vertical axis to visualize without obstruction one of the representative filaments (corresponding to the left virtual section in E). (Scale bar: 25 nm.)

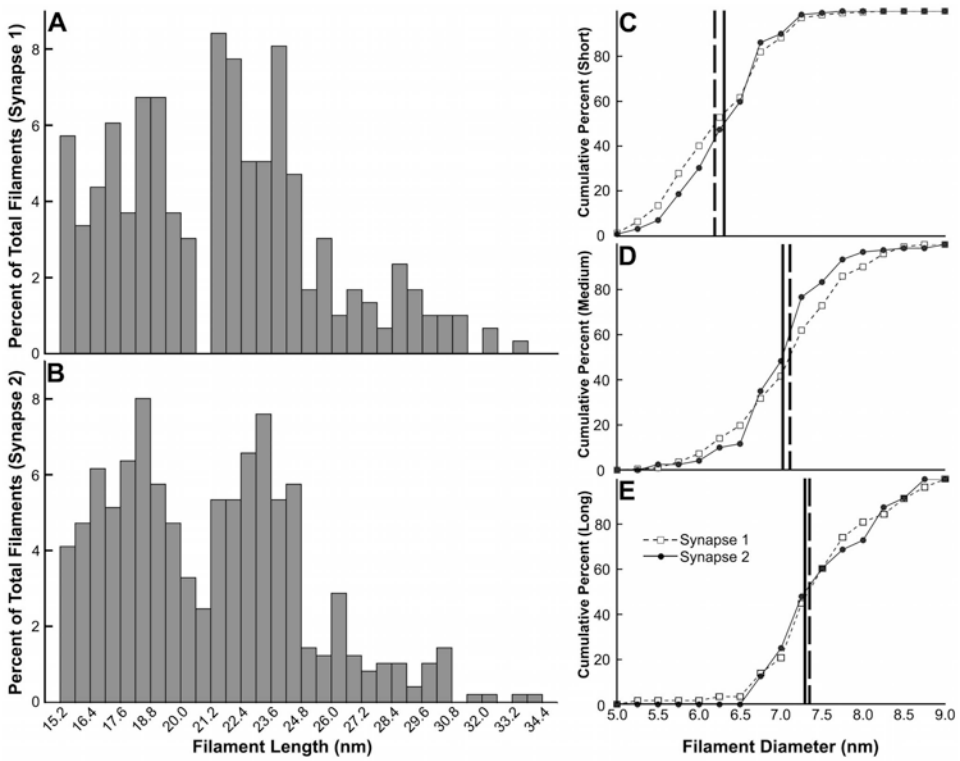

Figure 8. Postsynaptic filaments at two different GABAergic synapses exhibit congruent distributions of length and diameter

A, B, Frequency histograms of the lengths of rendered postsynaptic filaments at the synapses rendered first (A) and second (B). **C-E,** Cumulative frequency curves for the diameters of short (C), medium (D), and long filaments (E) at the two synapses rendered. Vertical lines indicate the diameter at which 50% of the filaments at the synapses rendered first (broken line) and second (solid line) are accounted for.

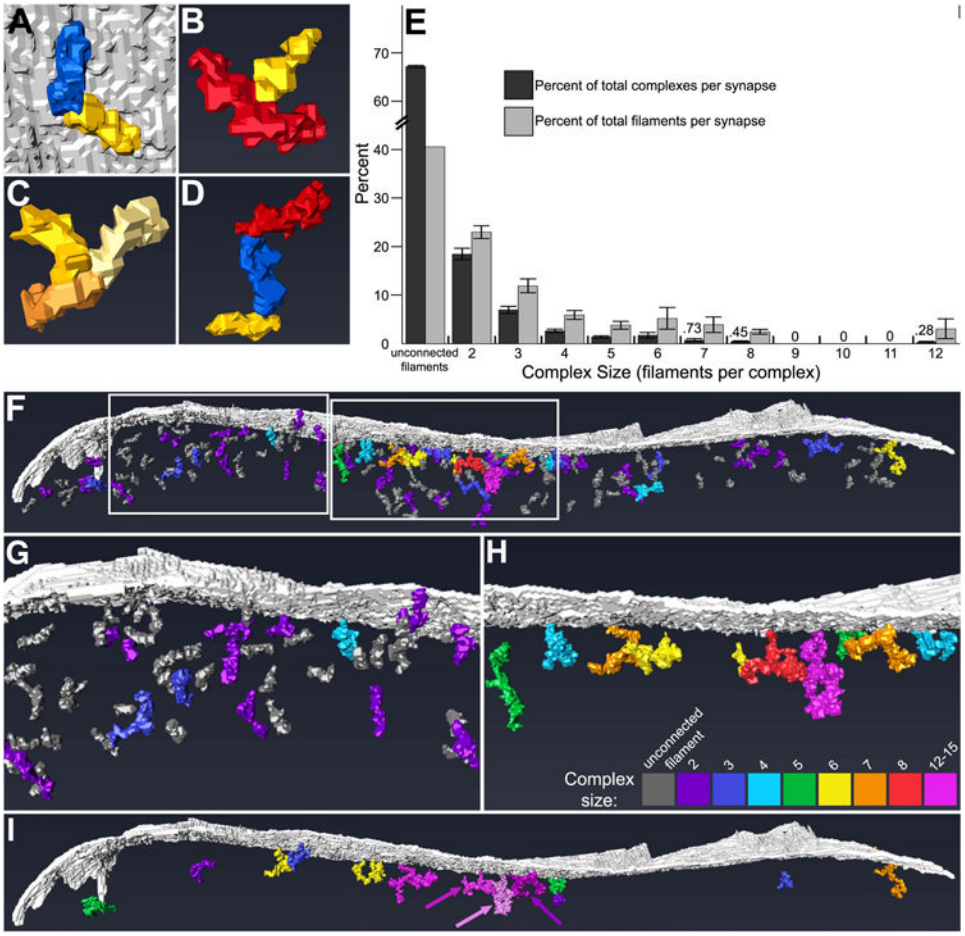

Figure 9. Filaments of the postsynaptic network at GABAergic synapses interconnect, forming higher-order complexes

A, Rendering of short filament (in yellow) and medium filament (blue) contacting tip-to-tip. Opposite tips of both filaments also contacted the postsynaptic membrane (gray). **B,** Rendering of long filament (red) contacting a short filament (yellow) middle-to-tip. **C,** Rendering of three short filaments (yellow, light yellow, and orange) contacting tip-to-tip-to-tip, apparently trimerized. **D,** Rendering of short filament (yellow) and medium filament (blue) contacting tip-to-tip, with medium filament also contacting long filament (red) tip-to-tip. Such contacts allow filaments to assemble into what appear to be molecular complexes. **E,** Bar graph of percent of total complexes composed of different numbers of filaments (dark bars) and percent of total filaments incorporated into complexes of different sizes (light bars) (mean ± SEM). Unassociated filaments and complexes composed of ≤3 filaments outnumbered complexes composed of ≥4 filaments. The majority of filaments were either unconnected to others or incorporated into complexes made of ≤3 filaments. Values for the smallest data points are provided above the corresponding bars. **F**-**H**, Rendering (side view) of the postsynaptic network and membrane (gray) showing the distribution of mono- and poly- filament structures throughout (F). The number of filaments incorporated into a given complex is indicated by its color (see key in H). Complexes composed of ≥4 filaments (cyan-pink) were preferentially located in the core of the postsynaptic network, while those composed of ≤3 filaments (dark gray-blue) were more predominant in the periphery and mantle, but some were also intercalated between the larger complexes of the core. G and H depict the left and right boxed areas in F, respectively, in

greater detail, with complexes composed of ≤3 filaments omitted for clarity in H. **I**, Rendering (side view) of the postsynaptic membrane (gray) and those complexes linked to others by irregular globules of electron-dense material; complexes that are not so linked have been excluded for clarity. The number of filaments incorporated into a given clutch of linked complexes (equal to the total number of filaments of its constituent complexes) is indicated by its color, according to the key in H. Arrows emphasize the distinction between three separate clutches rendered in pink, light pink, and dark pink.

Table 1

Antibody Specifications.

Antibody	Immunogen	Working dilution (EM)	Working dilution (LM)	Source
Anti-VIAAT	Amino acids 2-115 of rat VIAAT	1:100	1:500	Rabbit polyclonal (Synaptic Systems 131013)
Anti-GAD65	Affinity-purified GAD65 from rat brain	1:40	1:100	Mouse monoclonal (DSHB GAD-6)
Anti-gephyrin	Purified gephyrin from rat	1:50	1:250	Mouse monoclonal (Synaptic Systems 147021)
Anti-$GABA_AR$ α2	Amino acids 29-37 of rat $GABA_AR$α2 precursor protein	—	1:500	Rabbit polyclonal (Synaptic Systems 224103)

EM: electron microscopy, LM: light microscopy.

Table 2

Summary of Filament Dimensions and Connections by Class.

Filament Class	n_1[1]	n_2[1]	Length Range (nm)	Median Length ± MAD (nm)	Median Diameter ± MAD (nm)
Short	137	255	15.4 - 21.5	18.2 ± 1.2	6.3 ± 0.4[2]
Medium	122	174	21.5 - 25.4	23.8 ± 0.9	7.1 ± 0.4[2]
Long	46	58	25.7 - 35.0	27.8 ± 1.4	7.4 ± 0.5[2]

	% Connected to Another Filament ± SEM				
Filament Class	**At 1 Tip**	**At 2 Tips**	**At Middle**	**2× at 1 Tip**	**Total**
Short	43 ± 1	9 ± 2	9 ± 1[3]	10 ± 3	58 ± 1
Medium	43 ± 4	10 ± 2	15 ± 3	9 ± 2	58 ± 3
Long	40 ± 1	8 ± 3	20 ± 2[3]	10 ± 1	55 ± 4
All	43 ± 2	9 ± 1	12 ± 1	10 ± 1	57 + 1

[1] n_1 and n_2 refer to the number of filaments of each class in the first and second synapses rendered, respectively.

[2] P<0.001, three independent Mann-Whitney U tests with Bonferroni corrections.

[3] P<0.05, Pearson's chi-squared test of independence.